Proceedings of the 2007 American Control Conference
Marriott Marquis Hotel at Times Square
New York City, USA, July 11-13, 2007

Transient control of a Diesel engine airpath

Jonathan Chauvin, Gilles Corde, and Nicolas Petit

Abstract— **This article focuses on the control of a Diesel engine airpath during transients. The proposed control methodology uses a motion planning technique combined with an observer and two inner loop controllers. We extend and improve our previously published results by providing proof of *global* convergence and stability. The EU cycle serves as benchmark, and detailed experimental results (including transients in HCCI mode) are presented.**

I. INTRODUCTION

Performance and environmental requirements of Diesel engines have steadily increased over the last thirty years, which in turn has required an increase in the sophistication of employed control strategies. Advances in model based control over this period have been one of the keys in meeting the demands placed on modern combustion technologies. Lately, the Highly Premixed Combustion mode (HPC) – including Homogeneous Charge Compression Ignition (HCCI) – has become of major interest. It requires the use of high Exhaust Gas Recirculation (EGR) rates. The key idea is that the recirculated burned gas lower the in-cylinder temperature and dilute the air charge which reduces the emissions of nitrogen oxides. Simultaneous ignition in the whole combustion chamber is performed and controlled. Significant reduction in pollutants emission was proven in practice through numerous experiments (see [9], [18] for example). In that combustion mode, the core variable is the Burned Gas Rate (BGR) in the intake manifold. BGR offsets may cause misfires and malicious noises. In the HCCI combustion mode it is very high (40% or more). Accurate control of BGR can be achieved by controlling the whole airpath system: intake and exhaust manifolds, EGR loop and fresh air loop. This is the subject of the paper.

As studied in [13], [11], the airpath system of a turbocharged Diesel engine features coupled dynamics. The EGR acts as a discharge valve for the turbocharger. Most studies consider the following control setup: both intake pressure and intake air flow are closely controlled using EGR valve and Variable Geometry Turbocharger (VGT) using Gain scheduling PI controllers as in [17], [14], [16], using constructive Lyapunov control as in [7] or LPV formulation as in [8]. Controlling both intake and exhaust pressure has been exposed in [1]. All these studies prove the relevance of a multivariable control.

J. Chauvin (corresponding author) and G. Corde are with the Department of Engine Control in Institut Français du Pétrole, 1 et 4 Avenue de Bois Préau, 92852 Rueil Malmaison, France jonathan.chauvin@ifp.fr.

N. Petit is with the Centre Automatique et Systèmes, École des Mines de Paris, 60, bd St Michel, 75272 Paris, France

The control strategy we advocate is motion planning based. Since our first works [2] and [3], accuracy, robustness and range of operations points have been increasing and broadening. The final version we present here is able to address actual high EGR transients of benchmark EU cycle.

While in [3], we detailed the trajectory generation and the model inversion leading to an open loop control law u^{ol}, we did not explicitly take several important constraints into account at the trajectory generation stage. In [2], we exposed how to to generate feasible trajectories between steady points. Rather than only considering steady states, the challenge here is to address agressive transients that require a more global approach. The contribution of the paper is twofold. First, we prove the open loop global exponential stability of the dynamics and propose a globally exponentially converging observer. Finally, we prove the relevance of the approach on extensive experimental results.

The paper is organized as follows. In Section II we detail the system modelling. In Section III, we define the assumptions and constraints of the system and we prove some properties of the dynamics. In Section V, we detail an observer for the air path dynamics. Experimental results are reported on a 4 cylinder HCCI engine in Section VI.

II. INTAKE MANIFOLD MODELLING

Flows of fresh air (measured by the Manifold Air Flow) and from the EGR come into the intake manifold to be aspirated into the cylinders. In numerous references found in the literature (e.g. [15], [10]), mean value engine modelling approaches are considered. These use temporal and spatial averages of relevant temperatures, pressures and mass flow rates, and lead to a seven state reference model. The states are the intake and exhaust manifold pressure, temperature, and composition, and the turbocharger speed. Because complexity of the model impact on the control design, most authors usually consider a preliminary model reduction down to 3 states (see [17], [14], [8] or [7] for example). Further, we propose a reduction down to 2 states. Motivations are given in the following subsection.

A. Modelling assumptions

First of all, as it is standard in modelling the intake manifolds in spark-ignited engines (e.g. [4] and [5]), we neglect the temperature fluctuations. Out of the seven usual state variables, two are eliminated. The already discussed common model reduction (see [17], [14], [8] and [7]) consists of a three dimensional reference control model using the intake pressure, the exhaust pressure and the turbocharger speed as states. Composition dynamics are not taken into account

1-4244-0989-6/07/$25.00 ©2007 IEEE.

because the corresponding two states (intake and exhaust composition) are difficult to measure and are only weakly observable from the remaining three states. In our case, we use the Air/Fuel Ratio sensor located downstream the turbine. It is an image of the composition in the exhaust manifold. This major difference with usually considered setups suggests us to substitute the exhaust pressure dynamics with the intake composition dynamics. Finally, we neglect the turbocharger dynamics. The reason for this simplification is that the turbocharger speed dynamics is very slow compared to the pressure and composition dynamics. Finally, the turbocharger speed is modelled as a static function of the intake pressure P_{int} and the intake air flow D_{air}. These hypothesis yield a reduction down to a two dimensional state.

B. State space model

Two balance equations provide the model we build our work on. A nomenclature is presented in Table I.

1) Total mass balance in the intake manifold: Ideal gas law in the intake manifold leads to

$$P_{int}V_{int} = M_{int}RT_{int}$$

Assuming that variations of temperature are small, mass balance writes

$$\dot{P}_{int} = \frac{RT_{int}}{V_{int}}(D_{air} + D_{egr} - D_{asp}) \tag{1}$$

Classically (see [6] for exemple), we assume that the aspirated flow can be computed as

$$D_{asp} = \eta_{vol}(P_{int}, N_e)\frac{P_{int}}{RT_{int}}V_{cyl}\frac{N_e}{120}$$

where V_{cyl} is the cylinder volume. η_{vol} is the volumetric efficiency which is experimentally derived and, eventually, defined though a look-up table $\eta_{vol}(P_{int}, N_e)$.

2) Composition balance in the intake manifold: The burned gas ratio F_{int} is the fraction of burned gas in the intake manifold. It writes

$$F_{int} \triangleq 1 - \frac{M_{int,air}}{M_{int}}$$

The composition of the EGR (F_{egr}) is the composition in the exhaust manifold (F_{exh}) delayed by the transport through the EGR pipe. We consider that this delay is negligible, i.e. $F_{egr} = F_{exh}$. Mixing dynamics is modelled as

$$\dot{F}_{int} = \frac{RT_{int}}{P_{int}V_{int}}(D_{egr}(F_{exh} - F_{int}) - D_{air}F_{int}) \tag{2}$$

III. Air path system properties

TABLE I

NOMENCLATURE. I.M. REFERS TO THE INTAKE MANIFOLD.

Var.	Quantity	Unit	Symb.
P_{int}	Pressure in the i.m.	Pa	x_1
F_{int}	Fraction of burned gas in the i.m.	-	x_2
Θ_{egr}	Equivalent flow if EGR valve is full open	kg.s^{-1}	x_3
D_{air}	Manifold air flow	kg.s^{-1}	u_1
D_{egr}	EGR flow	kg.s^{-1}	u_2
S_{VGT}	VGT normalized position	-	v_1
S_{egr}	EGR valve effective area	-	v_2
T_{int}	Temperature in the i.m.	K	
M_{int}	Total mass in the i.m.	kg	
$M_{int,air}$	Air mass in the i.m.	kg	
V_{int}	Volume of the i.m.	L	
N_e	Engine Speed	rpm	
D_{asp}	Aspirated flow into the cylinders	kg.s^{-1}	
V_{cyl}	Volume of the cylinders	L	
γ	Ratio of specific heats	-	
F_{exh}	Fraction of burned gas in the e.m.	-	
R	Gas constant	J.(kgK)$^{-1}$	
η_{vol}	Volumetric efficiency	-	

A. Reference model

The air path is represented as the input output system (3) depicted in Figure 1 (right). We note

$$\alpha_{int} \triangleq \frac{RT_{int}}{V_{int}} \quad \text{and} \quad \beta_{int} \triangleq \frac{1}{RT_{int}}V_{cyl}\frac{N_e}{120}$$

Using (1) and (2), the reference dynamics reads

$$\begin{cases} \dot{x}_1 = & \alpha_{int}\left(u_1 + u_2 - \beta_{int}\eta_{vol}(x_1, N_e)x_1\right) \\ \dot{x}_2 = & \dfrac{\alpha_{int}}{x_1}\left(F_{exh}u_2 - (u_1 + u_2)x_2\right) \end{cases} \tag{3}$$

These equations correspond to the right part of Figure 1. This fully actuated system is linearizable by nonlinear static feedback: (x_1,x_2) are linearizing output. The motion planning problem is readily solved by imposing histories of (x_1,x_2) and computing corresponding inputs (see [3]).

B. Input constraints

1) Constraints on flow variables: By definition of input flows, input signals u_1 and u_2 are assumed positive. Moreover, to take physical limitations of the engine into account, the total input flow must be strictly positive and upper bounded. To summarize, we consider that there exists $(u_{min}, u_{max}) \in (\mathbb{R}^+ \setminus \{0\})^2$ such that

$$0 < u_{min} \leq u_1 + u_2 \leq u_{max}$$

2) Misfire avoidance: Our challenge here is to successfully pass the EU cycle. A necessary condition is to avoid misfires and the implied peaks in pollutant emissions. High EGR rates may cause these misfires. A simple strategy can address this issue. Conservatively, misfire avoidance can be guaranteed provided the following input constraints are satisfied

$$C(u) \triangleq F_{exh}\frac{u_2}{u_2 + u_1} \leq \overline{C} < 1$$

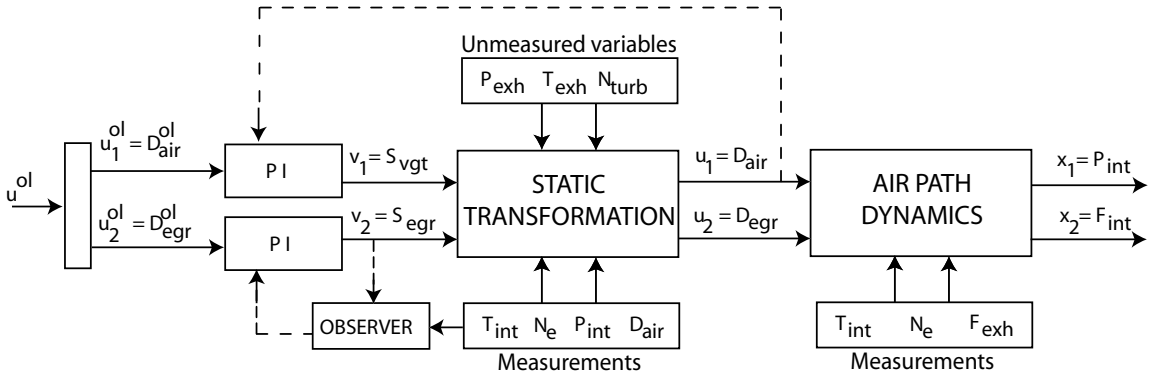

Fig. 1. Input/Output scheme of the air path dynamics and its associated control strategy.

3) Feasible inputs set: Combining the previously discussed constraints, the set of feasible inputs is defined as

$$\mathcal{U} \triangleq \begin{array}{l}\big\{(u_1,u_2)\in(\mathbb{R})^2/0<u_{min}\leq u_1+u_2\leq u_{max},\\ u_2\geq 0,\quad \text{and}\quad F_{exh}\frac{u_2}{u_2+u_1}\leq \bar{C}\big\}\end{array}$$

We note its boundary $\partial\mathcal{U}$. A typical representation of this convex set is given in Figure 2.

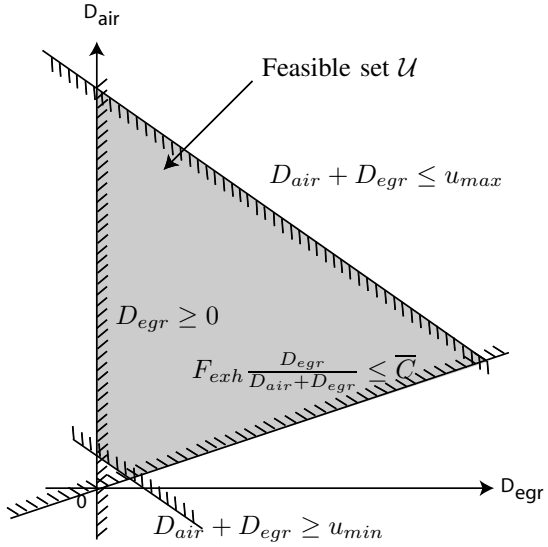

Fig. 2. Input constraints ($u_1=D_{air}, u_2=D_{egr}$), the feasible set $\mathcal{U}$ is represented in grey.

C. Assumptions

1) Boundedness of α_{int} and β_{int}: We assume that there exists $(\alpha_m,\alpha_M,\beta_m,\beta_M)\in(\mathbb{R}^+\setminus\{0\})^4$ such that

$$0<\alpha_m\leq\alpha_{int}\leq\alpha_M \quad\text{and}\quad 0<\beta_m\leq\beta_{int}\leq\beta_M$$

Equivalently, it is assumed that T_{int} and N_e are strictly positive and upper bounded (which, experimentally, is true).

2) Characteristics of the volumetric efficiency: It is assumed that the volumetric efficiency slowly varies w.r.t. the intake pressure x_1. We define the function h_{Ne}

$$\mathbb{R}^+\ni x_1\mapsto h_{Ne}(x_1)\triangleq\eta_{vol}(x_1,N_e)x_1 \tag{4}$$

We suppose that there exists a strictly positive constant $\underline{h}$ such that, for all $x_1>0$,

$$\frac{\partial h_{Ne}}{\partial x_1}(x_1)\geq\underline{h}>0$$

Experimentally, this assumption is actually easy to validate. It allows us to define

$$x_{1,m}\triangleq h_{Ne}^{-1}(\frac{u_{min}}{\beta_{int}}) \quad\text{and}\quad x_{1,M}\triangleq h_{Ne}^{-1}(\frac{u_{max}}{\beta_{int}})$$

Notice that, by construction, $x_{1,m}>0$, because h_{Ne} is a strictly increasing function with $h_{Ne}(0)=0$.

D. System properties

1) The state x is bounded: Consider the closed set $[x_{1,m},\ x_{1,M}]$. At the lower boundary, $x_{1,m}$, we have

$$\begin{aligned}\dot{x}_1&=\alpha_{int}\left(u_1+u_2-\beta_{int}h(x_{1,m})\right)\\&=\alpha_{int}(u_1+u_2-u_{min})\geq 0\end{aligned}$$

Similarly, at the upper boundary $x_{1,M}$, we have $\dot{x}_1\leq 0$. Along the boundaries of the domain $[x_{1,m},\ x_{1,M}]$, the vector field is pointing inside the domain. We can reformulate these inequalities into the following lemma

Lemma 1: For any initial condition such that $x_1(0)\in[x_{1,m},\ x_{1,M}]$, then, for all $t\geq 0$, the solution of (3) verifies $x_1(t)\in[x_{1,m},\ x_{1,M}]$.

Now, consider $[0,\bar{C}]$. Let $x_2=0$, then, we have $\dot{x}_2=\frac{\alpha_{int}}{x_1}F_{exh}u_2\geq 0$. Again, if $x_2=\bar{C}$,

$$\dot{x}_2=\frac{\alpha_{int}}{x_1}\left(F_{exh}u_2-(u_1+u_2)\bar{C}\right)\leq 0$$

because $F_{exh}\frac{u_2}{u_2+u_1}\leq\bar{C}$ since $u\in\mathcal{U}$. The following lemma holds

Lemma 2: For any initial condition such that $x_2(0)\in[0,\ \bar{C}]$, then, for all $t\geq 0$, the solution of (3) verifies $x_2(t)\in[0,\ \bar{C}]$.

At last, consider $\mathcal{X}\triangleq[x_{1,m},\ x_{1,M}]\times[0,\ \bar{C}]$. Using Lemma 1 and Lemma 2, we can now conclude and state

the following result.

Proposition 1: For any initial condition $x(0) = (x_1(0), x_2(0)) \in \mathcal{X}$, and for any control input u such that $u(t) \in \mathcal{U}$ for all $t \geq 0$, the solution $x(t)$ of (3) remains in $\mathcal{X}$ for all $t \geq 0$. The (functions) vector (x, u) is said to be a *feasible* trajectory.

2) System (3) *is globally exponentially open loop stable:* Let (x^r, u^r) be a feasible reference trajectory. Applying the open loop control law u^r to (3) with any initial condition $x(0) \in \mathcal{X}$, system (3) gives

$$\begin{cases} \dot{x}_1 = \alpha_{int}\left(u_1^r + u_2^r - \beta_{int} h_{Ne}(x_1)\right) \\ \dot{x}_2 = \dfrac{\alpha_{int}}{x_1}\left(F_{exh} u_2^r - (u_1^r + u_2^r) x_2\right) \end{cases} \tag{5}$$

Let $\tilde{x} = x^r - x$, the error between the reference state and the solution of (5) with $x(0) \in \mathcal{X}$ as initial condition. We get

$$\begin{cases} \dot{\tilde{x}}_1 = -\alpha_{int}\beta_{int}\left(h_{Ne}(x_1^r) - h_{Ne}(x_1)\right) \\ \dot{\tilde{x}}_2 = -\dfrac{\alpha_{int}}{x_1 x_1^r}\left(F_{exh} u_2^r - (u_1^r + u_2^r) x_2\right)\tilde{x}_1 \\ \qquad\qquad - \alpha_{int}\dfrac{u_1^r + u_2^r}{x_1^r}\tilde{x}_2 \end{cases} \tag{6}$$

Exponential convergence of $\tilde{x}$ toward 0 can be studied by exploiting the cascade structure of equations (6).

First, we focus on the $\tilde{x}_1$-dynamics. The differentiation of the squared norm of $\tilde{x}_1$ leads to

$$\begin{aligned} \frac{d}{dt}\left(\tilde{x}_1^2\right) &= -2\alpha_{int}\beta_{int}\left(h_{Ne}(x_1) - h_{Ne}(x_1^r)\right)\tilde{x}_1 \\ &\leq -2\tau_m \tilde{x}_1^2 \end{aligned}$$

where $\tau_m \triangleq \alpha_m \beta_m \underline{h}$. Thus, we have

$$\forall t \in \mathbb{R}^+, \quad |\tilde{x}_1(t)| \leq e^{-\tau_m t}\,|\tilde{x}_1(0)| \tag{7}$$

Some easy rewriting of the $\tilde{x}_2$-dynamics leads to

$$\dot{\tilde{x}}_2 = -\phi(t)\tilde{x}_2 + \psi(t) \tag{8}$$

where

$$\begin{cases} \psi(t) \triangleq -\dfrac{\alpha_{int}}{x_1 x_1^r}\left(F_{exh} u_2^r - (u_1^r + u_2^r) x_2\right)\tilde{x}_1 \\ \phi(t) \triangleq \alpha_{int}\dfrac{u_1^r + u_2^r}{x_1^r} \end{cases}$$

The analytic solution of (8) is

$$\begin{aligned} \tilde{x}_2(t) = &\exp\left(-\int_0^t \phi(s)ds\right)\tilde{x}_2(0) \\ &+ \int_0^t \exp\left(-\int_s^t \phi(\tau)d\tau\right)\psi(s)ds \end{aligned} \tag{9}$$

From Proposition 1, $x \in \mathcal{X}$. Then, it follows that the function ψ is bounded because u^r, x^r,α_{int}, F_{exh} are. Yet, from (7), we have

$$\forall t \geq 0, \quad |\psi(t)| \leq \Psi e^{-\tau_m t}$$

where $\Psi \triangleq 2\frac{\alpha_M}{x_{1,M}^2} u_{max} \bar{C}\,|\tilde{x}_1(0)|$. The function ϕ is strictly positively bounded because α_{int}, x^r and u^r are, i.e.

$$\forall t \geq 0, \quad 0 < \underline{\phi} \triangleq \min\{\frac{\tau_m}{2}, \alpha_m \frac{u_{min}}{x_{1,M}}\} \leq \phi(t)$$

These last two inequalities yield

$$|\tilde{x}_2(t)| \leq \left(|\tilde{x}_2(0)| + \frac{\Psi}{\tau_m - \underline{\phi}}\right) e^{-\underline{\phi} t} + \frac{\Psi}{\tau_m - \underline{\phi}} e^{-\tau_m t}$$

Together with (7), this prove that the error $\tilde{x}$ is globally exponentially stable. The following result holds.

Proposition 2: Consider a feasible reference trajectory (x^r, u^r). Feed (3) with the control input u^r. Then, the error state $x - x^r$ globally exponentially converges toward 0.

This proposition is the key to understanding our approach. Provided chosen control values are feasible (i.e. belong to $\mathcal{U}$), it is sufficient to use them as inputs in the airpath system to exponentially reach a desired reference trajectory. For implementation, this strategy has to be complemented by an estimation technique to recover unmeasured variables.

IV. Control strategy

The control strategy we propose is pictured in Figure 3. It comprises 4 sub procedures:

- From the driver's torque demand to x^{sp}: set point computations through static maps (first two blocks in Figure 3).
- From x^{sp} to x^{mp}: trajectory generation for the state x.
- From x^{mp} to u^{mp}: model inversion, generation of the open loop control laws.
- From u^{mp} to u^{ol}: projection onto the feasible set $\mathcal{U}$.

The set points maps are calibrated at steady state. The calibration is a tradeoff between consumption, pollutants, and noise. In [3], we detail the trajectory generation and the model inversion leading to an open loop control law u^{ol}.

Proposition 2 proves global open loop stability. If the proposed control is feasible, then $u^{\mathrm{mp}}(t) = u^{\mathrm{ol}}(t)$ for all $t \geq 0$ and, neglecting possible perturbations, the transient is perfectly achieved. The feedback loop guarantees the tracking of the planned input values despite various uncertainties. This feedback corresponds to the left part of Figure 1. There are two feedback loop :

- Feedback on u_1 with v_1. We use a PI controller to zero the error between the reference air flow u_1^r and the measured air flow u_1.
- Feedback on u_2 with v_2. We use a PI controller to zero the error between the reference EGR flow u_2^r and the estimated EGR flow u_2.

The EGR flow is not measured, we have to estimate it. This is the purpose of next section.

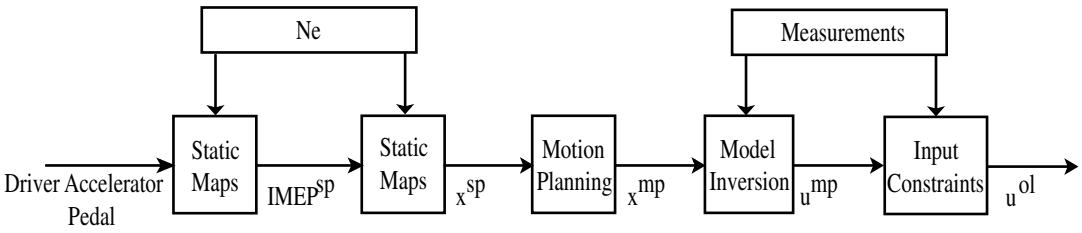

Fig. 3. Motion planning scheme: from torque demand to feedforward control.

V. Air path observer

As pictured in Figure 1, the real control variables are not (u_1, u_2) but rather (v_1, v_2). The airpath dynamics has (u_1, u_2) as physical inputs but these are not directly actuated. One can act upon (v_1, v_2) which uniquely define (u_1, u_2), provided several variables (see again Figure 1) are known. Some of the required variables are measured (T_{int},N_e,P_{int},D_{air}), while some are not (P_{exh}, T_{exh},N_{turb}). In the following, we explain how to recover the unmeasured variables. This is necessary to eventually close the loop on the (v_1, v_2) input channels.

As described in [6], a common model is

$$u_2 = v_2 \frac{P_{exh}}{\sqrt{RT_{exh}}} \sqrt{\frac{2\gamma}{\gamma - 1} \left(p_r^{\frac{2}{\gamma}} - p_r^{\frac{\gamma+1}{\gamma}} \right)}$$

where $p_r = \max\{\frac{P_{int}}{P_{exh}}, (\frac{2}{\gamma+1})^{\frac{\gamma}{\gamma+1}}\}$. These two values describe both subsonic and choked EGR flow. In this model, numerous variables are not measured. For example, the exhaust pressure P_{exh} and temperature T_{exh} are not easily available on a commercial engine. Note

$$\Theta_{egr} \triangleq \frac{P_{exh}}{\sqrt{RT_{exh}}} \sqrt{\frac{2\gamma}{\gamma - 1} \left(p_r^{\frac{2}{\gamma}} - p_r^{\frac{\gamma+1}{\gamma}} \right)}$$

This unknown variable needs to be reconstructed to evaluate the EGR flow u_2.

We assume that with a fixed distribution, the internal gas locked in the cylinder are negligible. Under these assumptions, we now present a reference model dynamics and propose an observer. The observer design follows [3]. Here, exponential convergence of the observer is proven using Lyapunov arguments.

A. Reference model

Let $x = \begin{bmatrix} P_{int} & F_{int} & \Theta_{egr} \end{bmatrix}^T \in \mathbb{R}^3$ be the state and $y = P_{int}$ the measurement. Using (3), the reference dynamics reads

$$\begin{cases} \dot{x}_1 = \alpha_{int} \left(u_1 + v_2 x_3 - \beta_{int} \eta_{vol}(x_1, N_e) x_1 \right) \\ \dot{x}_2 = \dfrac{\alpha_{int}}{x_1} \left(F_{exh} v_2 x_3 - (u_1 + v_2 x_3) x_2 \right) \\ \dot{x}_3 = 0 \end{cases}, \quad y = x_1 \tag{10}$$

B. Observer Design

The observer dynamics are

$$\begin{cases} \dot{\hat{x}}_1 = \alpha_{int} \left(u_1 + v_2 \hat{x}_3 - \eta_{vol}(y, N_e) \beta_{int} \hat{x}_1 \right) \\ \qquad\qquad - L_1(\hat{x}_1 - y) \\ \dot{\hat{x}}_2 = \dfrac{\alpha_{int}}{y} \left(F_{exh} v_2 \hat{x}_3 - (u_1 + v_2 \hat{x}_3) \hat{x}_2 \right) \\ \dot{\hat{x}}_3 = -L_3(\hat{x}_1 - y) \end{cases} \tag{11}$$

with L_1 and L_3 strictly positive variables. One can notice that (11) is a copy of (10) with additive tracking terms. Unknowns are partially substituted with output measurements. Variable gains L_1 and L_3 are chosen as follows

$$L_1 = (l_1 - \eta_{vol}(y, N_e)) \alpha_{int} \beta_{int}, \quad L_3 = l_3 \alpha_{int} u$$

where l_1 and l_3 are positive constants. Noting the state-error $\tilde{x} \triangleq x - \hat{x}$, the error system writes under the triangular form (12)-(13)

$$\begin{cases} \dot{\tilde{x}}_1 = \alpha_{int} \left(v_2 \tilde{x}_3 - l_1 \beta_{int} \tilde{x}_1 \right) \\ \dot{\tilde{x}}_3 = -l_3 \alpha_{int} \tilde{x}_1 v_2 \end{cases} \tag{12}$$

$$\begin{aligned} \dot{\tilde{x}}_2 = & \frac{\alpha_{int}}{y} \left(F_{exh} v_2 \tilde{x}_3 - (u_1 + v_2 \hat{x}_3) \tilde{x}_2 \right) \\ & + \frac{\alpha_{int}}{y} (F_{exh} - x_2) \tilde{x}_3 \end{aligned} \tag{13}$$

C. Convergence analysis

To investigate convergence of the proposed observer, we assume that $v_2 > 0$. This last assumption is not restrictive since, when v_2 equals 0, the EGR valve is completely closed and that, consequently, it can be undoubtedly inferred that the EGR flow u_2 is equal to 0. From this assumption, the convergence proof is divided in two parts. It exploits the cascade structure of the error dynamics (12)-(13).

1) $(\tilde{x}_1, \tilde{x}_3)$-dynamics: the $(\tilde{x}_1, \tilde{x}_3)$-dynamics is independent of $\tilde{x}_2$. Its dynamics writes

$$\begin{bmatrix} \dot{\tilde{x}}_1 \\ \dot{\tilde{x}}_3 \end{bmatrix} = A_{int}(t) \begin{bmatrix} \tilde{x}_1 \\ \tilde{x}_3 \end{bmatrix}$$

$$\text{where} \quad A_{int}(t) \triangleq \begin{bmatrix} -l_1 \alpha_{int} \beta_{int} & \alpha_{int} v_2 \\ l_2 \alpha_{int} v_2 & 0 \end{bmatrix}$$

A Lyapunov function candidate is

$$V(\tilde{x}) = \frac{1}{2} \left(\tilde{x}_1^2 + \frac{1}{l_3} \tilde{x}_3^2 \right) \tag{14}$$

First of all, $V(0) = 0$, and $\forall \tilde{x} \in \mathbb{R}^2 \setminus \{0\}$, $V(\tilde{x}) > 0$. Differentiation yields

$$\dot{V}(\tilde{x}) = \tilde{x}_1\dot{\tilde{x}}_1 + \frac{1}{l_3}\tilde{x}_3\dot{\tilde{x}}_3 = -\alpha_{int}\beta_{int}l_1\tilde{x}_1^2$$

Yet, α_{int} and β_{int} are bounded. This leads to $\dot{V}(\tilde{x}) \leq -\alpha_m\beta_m l_1\tilde{x}_1^2$. Since α_{int} and β_{int} are time varying, we can not directly apply LaSalle's invariance principle to conclude. Nevertheless, since $\dot{V}(\tilde{x}) \leq 0$ in $\Omega_r = \{\tilde{x}_f = [\tilde{x}_{1,f} \quad \tilde{x}_{3,f}]^T \in \mathbb{R}^2 / V(\tilde{x}_f) < r\} \subset \mathbb{R}^2$, $t \mapsto V(\tilde{x}(t))$ is a decreasing function. Since $V(\tilde{x})$ is continuous on the compact Ω_r, it is bounded from bellow on Ω_r. Therefore, $V(\tilde{x}(t))$ has a limit when $t \to +\infty$. Moreover,

$$\begin{aligned} V(0) \geq V(0) - V(\tilde{x}(t)) &= -\int_0^t \dot{V}(\tilde{x}(\tau))d\tau \\ &\geq \alpha_m\beta_m l_1 \int_0^t \tilde{x}_1^2(\tau)d\tau \end{aligned}$$

and so $\tilde{x}_1$ is square integrable. As $\tilde{x}_1$ is uniformly continuous, $\tilde{x}_1(t)$ tends to 0 as $t \to +\infty$. Further, $\tilde{x}_1$ and $\tilde{x}_3$ are uniformly continuous and bounded (because $V(\tilde{x}) \leq V(0)$) yielding $\dot{\tilde{x}}_1$ is uniformly continuous and bounded. Finally, $\dot{\tilde{x}}$ is uniformly continuous and $\lim_{t\to+\infty} \tilde{x}_1(t) = 0$, then from Barbalat's lemma (see e.g. [12])

$$\lim_{t\to+\infty} \dot{\tilde{x}}_1(t) = 0$$

Thus, $\lim_{t\to+\infty} \tilde{x}_3(t) = 0$ and the equilibrium point is uniformly asymptotically stable. However, the dynamics is linear. Thus, this implies that $\tilde{x}_1$ and $\tilde{x}_3$ are exponentially stable (see [12, Theorem 4.11]). In other words there exists $(\tau_{int}, \lambda_{int}) \in (\mathbb{R}^+ \setminus \{0\})^2$ s. t., $\forall t \in \mathbb{R}^+$,

$$|\tilde{x}_1(t)| \leq \tau_{int}e^{-\lambda_{int}t} \quad \text{and} \quad |\tilde{x}_3(t)| \leq \tau_{int}e^{-\lambda_{int}t} \qquad (15)$$

2) $\tilde{x}_2$-dynamics: On the other hand, the $\tilde{x}_2$ dynamics writes

$$\dot{\tilde{x}}_2 = -a_{int}(t)\tilde{x}_2 + b_{int}(t) \qquad (16)$$

where

$$\begin{cases} a_{int}(t) \triangleq \dfrac{\alpha_{int}}{y}(u_1 + v_2\hat{x}_3) \\ b_{int}(t) \triangleq \dfrac{\alpha_{int}}{y}(F_{exh} - x_2)v_2\tilde{x}_3 \end{cases}$$

The analytical solution of (16) is

$$\begin{aligned} \tilde{x}_2(t) = &\exp\left(-\int_{t_0}^t a_{int}(s)ds\right)\tilde{x}_2(t_0) + \\ &\int_{t_0}^t \exp\left(-\int_s^t a_{int}(\tau)d\tau\right) b_{int}(s)ds \end{aligned} \qquad (17)$$

From Proposition 1, x is bounded. Then, it follows that the function b_{int} is bounded because v, α_{int}, $\tilde{x}_3$ are. We have

$$\forall t \in \mathbb{R}^+, \quad |b_{int}(t)| \leq Be^{-\lambda_{int}t}$$

where $B \triangleq \frac{\alpha_M}{x_{1,m}}\tau_{int}$. Moreover, as $|\tilde{x}_3(t)| \leq \tau_{int}e^{-\lambda_{int}t}$, there must exist $t_0 \triangleq \max\{0, \frac{1}{\lambda_{int}}\log(\frac{3|\tilde{x}_3(0)|}{2u_{min}})\}$ such that

$$\forall t \geq \tau_0, \quad a_{int}(t) \geq \underline{a} \triangleq \min\{\frac{\lambda_{int}}{2}, \frac{\alpha_M}{x_{1,m}}\frac{u_{min}}{3}\} > 0$$

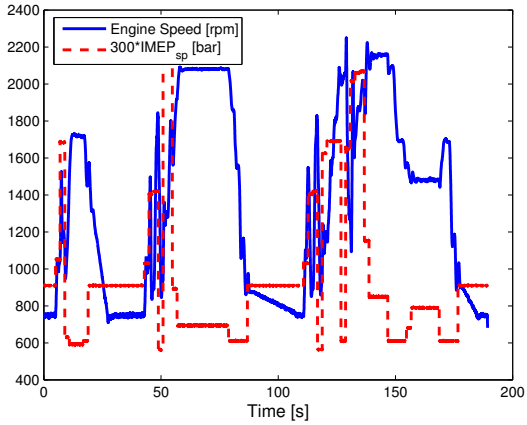

Fig. 4. Engine speed/ Torque trajectory on the ECE cycle.

These last two inequalities yield

$$\begin{aligned} |\tilde{x}_2(t)| \leq &\left(|\tilde{x}_2(t_0)| + \frac{B}{\lambda_{int} - \underline{a}}\right)e^{-\underline{a}(t-t_0)} \\ &+ \frac{B}{\lambda_{int} - \underline{a}}e^{-\lambda_{int}(t-t_0)} \end{aligned}$$

Together with (15), this prove that the error $\tilde{x}$ is globally exponentially stable. The following result holds.

Proposition 3: Assuming that $v_2 > 0$, there exists $t_0 \triangleq \max\{0, \frac{1}{\lambda_{int}}\log(\frac{3|\tilde{x}_3(0)|}{2u_{min}})\}$ such that, for $t \geq t_0$, the error state $\tilde{x}$ exponentially converge towards 0.

VI. Experimental results

The control was tested on the driving cycle of the (ECE) EU cycle with a 4 cylinder HCCI engine (see [18] for more detail on the engine). This driving cycle is very challenging for engine control systems. Indeed, this driving cycle has a highly varying torque demand. Moreover, 85% of the cycle is in the HCCI combustion mode.

The same tuning parameters were kept all along the driving cycle. The engine speed/IMEP demand is given in Figure 4. The BGR is well tracked as can be seen in Figure 5. The dynamics is fast and the over/undershoot are very small. This prevents misfires and malicious noises. Contrary to standard Diesel engines, in HCCI mode operated engines, the fuel/air mixture is premixed and ignition is controlled by the kinetics of the process. The main parameter available to control is the BGR. Accurate BGR tracking allow the HCCI engine to avoid stall and keep pollutant and noise below an acceptable level.

The air and EGR flows set points are presented along with closed-loop trajectory in Figures 6 and 7. The EGR flow is almost perfectly tracked. The air flow tracking is good but a little bit slow during large transient. This is due to the neglected turbocharger dynamics. In summary, the results are good, even for large transients.The planned trajectory is well tracked. High pressure set points are more difficult to reach

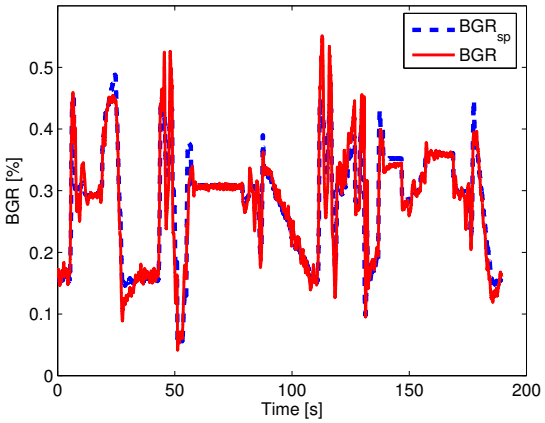

Fig. 5. Experimental results on the ECE driving cycle: BGR histories. Dashed : set point, solid: closed-loop trajectory.

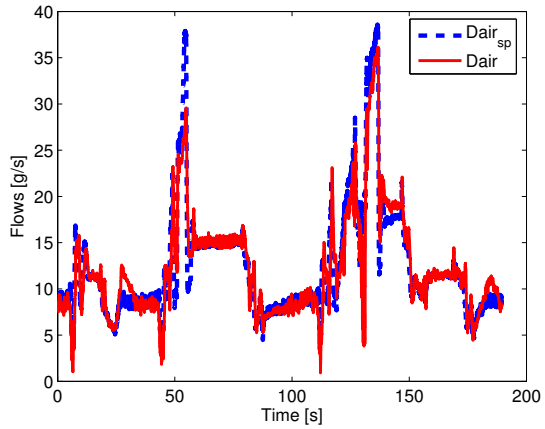

Fig. 6. Experimental results on the ECE driving cycle: Air flow histories. Dashed : set point, solid: closed-loop trajectory.

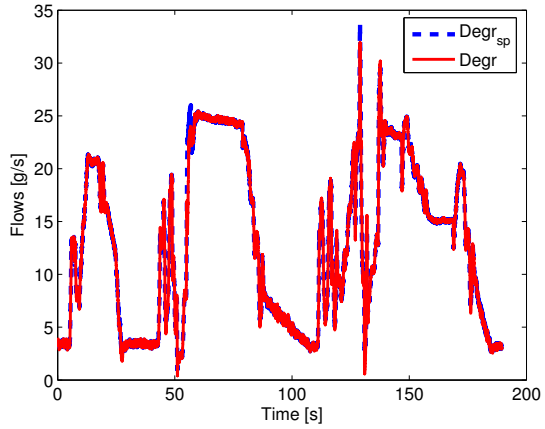

Fig. 7. Experimental results on the ECE driving cycle: EGR flow histories. Dashed : set point, solid: closed-loop trajectory.

due to the turbocharger inertia and friction. Meanwhile, it is not needed to accurately track the intake pressure because, for pollutant reduction purposes, only BGR needs to be closely controlled provided an upper limit on the Air-Fuel Ratio is not reached. The errors on the intake pressure only yield very small errors in the torque production. These results stress the relevance of the proposed control strategy.

ACKNOWLEDGMENTS

The authors would like to thank Lino Guzzella and Carlos Canudas-de-Witt for the fruitful discussions on airpath dynamics properties and estimation problem.

REFERENCES

[1] M. Ammann, N. Fekete, L. Guzzella, and A. Glattfelder, "Model-based control of the VGT and EGR in a turbocharged common-rail Diesel engine: theory and passenger car implementation," in *Proc. of the SAE Conference*, no. 2003-01-0357, 2003.

[2] J. Chauvin, G. Corde, and N. Petit, "Constrained motion planning for the airpath of a Diesel HCCI engine," in *Proc. of the IEEE Conf. Decision and Control*, 2006.

[3] J. Chauvin, G. Corde, N. Petit, and P. Rouchon, "Experimental motion planning in airpath control for HCCI engine," in *Proc. of the IEEE Conf. American Control Conference*, 2006.

[4] J. Grizzle, J. Cook, and W. Milam, "Improved air charge estimation for transient air fuel ratio control," in *Proc. of the IEEE Conf. American Control Conference*, 1994.

[5] E. Hendricks, A. Chevalier, M. Jensen, S. Sorenson, D. Trumpy, and J. Asik, "Modelling of the intake manifold filling dynamics," in *Proc. of the SAE Conference*, 1996.

[6] J. Heywood, *Internal Combustion Engine Fundamentals*. McGraw-Hill, Inc, 1988.

[7] M. Janković and I. Kolmanovsky, "Constructive Lyapounov control design for turbocharged Diesel engines," *IEEE Transactions on Control Systems Technology*, vol. 8, pp. 288–299, 2000.

[8] M. Jung and K. Glover, "Comparison of uncertainty parameterisations for H-infinity robust control of turbocharged Diesel engines," *Control Engineering Practice*, vol. 13, pp. 15–25, 2005.

[9] J. Kahrstedt, K. Behnk, A. Sommer, and T. Wormbs, "Combustion processes to meet future emission standards," in *Motortechnische Zeitschrift*, 2003, pp. 1417–1423.

[10] M. Kao and J. Moskwa, "Turbocharged Diesel engine modeling for nonlinear engine control and estimation," *ASME Journal of Dynamic Systems, Measurement and Control*, vol. 117, 1995.

[11] ——, "Turbocharged Diesel engine modelling for nonlinear engine control and estimation," *ASME Journal of Dynamic Systems, Measurements and Control*, vol. 117, 1995.

[12] H. Khalil, *Nonlinear Systems*. Prentice-Hall, Inc., 1992.

[13] I. Kolmanovsky, A. Stefanopoulou, P. Moraal, and M. van Nieuwstadt, "Issues in modelling and control of intake flow in variable geometry turbocharged engines," in *Proc of the 18th IFIP Conference on System Modelling and Optimization*, 1997.

[14] A. Stefanopoulou, I. Kolmanovsky, and J. Freudenberg, "Control of variable geometry turbocharged Diesel engines for reduced emissions," *IEEE Transactions on Control Systems Technology*, vol. 8, pp. 733–745, 2000.

[15] S.-C. Tsai and M. Goyal, "Dynamic turbocharged Diesel engine model for control analysis and design," in *Proc. of the SAE Conference*, 1986.

[16] M. van Nieuwstadt, I. Kolmanovsky, P. Moraal, A. Stefanopoulou, and M. Janković, "Experimental comparison of EGR-VGT control schemes for a high speed Diesel engine," *Control System Magazine*, vol. 20, pp. 63–79, 2000.

[17] M. van Nieuwstadt, P. Moraal, I. Kolmanovsky, A. Stefanopoulou, P. Wood, and M. Criddle, "Decentralized and multivariable designs for EGR-VGT control of Diesel engine," in *Proc of the 2nd IFAC Workshop on Advances in Automotive Control*, 1998.

[18] B. Walter and B. Gatellier, "Near zero NO_x emissions and high fuel efficiency diesel engine: the NADI^{TM} concept using dual mode combustion," vol. 58, no. 1, pp. 101–114, 2003.